Study of Large Hemispherical Photomultiplier Tubes for the ANTARES Neutrino Telescope

The ANTARES Collaboration

J.A. Aguilar [a], A. Albert [b], F. Ameli [c], P. Amram [d], M. Anghinolfi [e], G. Anton [f], S. Anvar [g], F.E. Ardellier-Desages [g], E. Aslanides [h], J-J. Aubert [h], D. Bailey [i], S. Basa [h], M. Battaglieri [e], Y. Becherini [j], R. Bellotti [k], J. Beltramelli [g], V. Bertin [h], M. Billault [h], R. Blaes [b], F. Blanc [ℓ], N. de Botton [g], J. Boulesteix [d], M.C. Bouwhuis [m], C.B. Brooks [i], S.M. Bradbury [n], R. Bruijn [m], J. Brunner [h], G.F. Burgio [o], F. Cafagna [k], A. Calzas [h], A. Capone [c], L. Caponetto [o], E. Carmona [a], J. Carr [h], S.L. Cartwright [p], E. Castorina [q], V. Cavasinni [q], S. Cecchini [j,r], P. Charvis [s], M. Circella [k], C. Colnard [m], C. Compère [t], R. Coniglione [y], S. Cooper [i], P. Coyle [h], S. Cuneo [e], G. Damy [t], R. van Dantzig [m], A. Deschamps [s], C. De Marzo [k], D. Denans [g], J-J. Destelle [h], R. De Vita [e], B. Dinkelspiler [h], C. Distefano [y], J-F. Drogou [u], F. Druillole [g], J. Engelen [m], J-P. Ernenwein [b], E. Falchini [q], S. Favard [h], F. Feinstein [h *], S. Ferry [v], D. Festy [t], V. Flaminio [q], J. Fopma [i], J-L. Fuda [ℓ], J-M. Gallone [v], G. Giacomelli [j], N. Girard [b], P. Goret [g], K. Graf [f], G. Hallewell [h], B. Hartmann [f], A. Heijboer [m], Y. Hello [s], J.J. Hernández-Rey [a], G. Herrouin [u], J. Hößl [f], C. Hoffmann [v], J. R. Hubbard [g], M. Jaquet [h], M. de Jong [m], F. Jouvenot [g], A. Kappes [f], T. Karg [f], S. Karkar [h], M. Karolak [g], U. Katz [f], P. Keller [h], P. Kooijman [m], E.V. Korolkova [p], A. Kouchner [w,g], W. Kretschmer [f], S. Kuch [f], V.A. Kudryavtsev [p], H. Lafoux [g], P. Lagier [h], R. Lahmann [f], P. Lamare [g], J-C. Languillat [g], H. Laschinsky [f], L. Laubier [ℓ], T. Legou [h], Y. Le Guen [t], H. Le Provost [g], A. Le Van Suu [h], L. Lo Nigro [o], D. Lo Presti [o], S. Loucatos [g], F. Louis [g], V. Lyashuk [x], M. Marcelin [d], A. Margiotta [j], C. Maron [s], A. Massol [u], R. Masullo [c], F. Mazéas [t], A. Mazure [d], J.E. McMillan [p], E. Migneco [y], C. Millot [ℓ], A. Milovanovic [n],

* Now at: Groupe d'Astroparticules de Montpellier, UMR 5139-UM2/IN2P3-CNRS, Université Montpellier II, Place Eugène Bataillon - CC85, 34095 Montpellier Cedex 5, France

F. Montanet [h], T. Montaruli [k †], J-P. Morel [t], M. Morganti [q], L. Moscoso [g], M. Musumeci [y], C. Naumann [f], M. Naumann-Godo [f], E. Nezri [h], V. Niess [h], G.J. Nooren [m], P. Ogden [n], C. Olivetto [v], N. Palanque-Delabrouille [g], R. Papaleo [y], P. Payre [h], C. Petta [o], P. Piattelli [y], J-P. Pineau [v], J. Poinsignon [g], V. Popa [j,z], R. Potheau [h], T. Pradier [v], C. Racca [v], G. Raia [y], N. Randazzo [o], D. Real [a], B.A.P. van Rens [m], F. Réthoré [h], G. Riccobene [y], V. Rigaud [u], M. Ripani [e], V. Roca-Blay [a], J-F. Rolin [t], M. Romita [k], H.J. Rose [n], A. Rostovtsev [x], M. Ruppi [k], G.V. Russo [o], Y. Sacquin [g], F. Salesa [a], K. Salomon [f], S. Saouter [g], P. Sapienza [y], R. Shanidze [f], J-P. Schuller [g ‡], W. Schuster [i], I. Sokalski [k], M. Spurio [j], T. Stolarczyk [g], D. Stubert [b], M. Taiuti [e], L.F. Thompson [p], S. Tilav [i], P. Valdy [u], V. Valente [c], B. Vallage [g], P. Vernin [g], J. Virieux [s], G. de Vries [m], P. de Witt Huberts [m], E. de Wolf [m], D. Zaborov [x], H. Zaccone [g], V. Zakharov [x], J.D. Zornoza [a §], J. Zúñiga [a]

[a] *IFIC – Instituto de Física Corpuscular, Edificios Investigación de Paterna, CSIC – Universitat de València, Apdo. de Correos 22085, 46071 Valencia, Spain*

[b] *GRPHE – Groupe de Recherche en Physique des Hautes Energies, Université de Haute Alsace, 61 Rue Albert Camus, 68093 Mulhouse Cedex, France*

[c] *Dipartimento di Fisica dell'Università "La Sapienza" e Sezione INFN, P.le Aldo Moro 2, 00185 Roma, Italy*

[d] *LAM – Laboratoire d'Astrophysique de Marseille, CNRS/INSU - Université de Provence Aix-Marseille I, Traverse du Siphon – Les Trois Lucs, BP 8, 13012 Marseille Cedex 12, France*

[e] *Dipartimento di Fisica dell'Università e Sezione INFN, Via Dodecaneso 33, 16146 Genova, Italy*

[f] *University of Erlangen,Friedrich-Alexander Universität Erlangen-Nürnberg, Physikalisches Institut,Erwin-Rommel-Str. 1, 91058 Erlangen, Germany*

† Now at: University of Wisconsin, Dep. of Physics, Chamberlin Hall, Madison, WI 53706, USA

‡ Now at: Istituto di Fisica Nucleare, Sezione di Roma, Piazzale Aldo Moro 2, 00185, Italy

§ Corresponding author.

E-mail address: zornoza@ific.uv.es

Now at: University of Wisconsin, Space Science & Engineering Center, 222 W Washington Ave., Madison, WI 53703, USA

[g] *DSM/DAPNIA – Direction des Sciences de la Matière, Département d'Astrophysique de Physique des Particules de Physique Nucléaire et de l'Instrumentation Associée, CEA/Saclay, 91191 Gif-sur-Yvette Cedex, France*

[h] *CPPM – Centre de Physique des Particules de Marseille, CNRS/IN2P3 Université de la Méditerranée Aix-Marseille II, 163 Avenue de Luminy, Case 907, 13288 Marseille Cedex 9, France*

[i] *University of Oxford, Department of Physics, Denys Wilkinson Building, Keble Road, Oxford OX1 3RH, United Kingdom*

[j] *Dipartimento di Fisica dell'Università e Sezione INFN, Viale Berti Pichat 6/2, 40127 Bologna, Italy*

[k] *Dipartimento Interateneo di Fisica e Sezione INFN, Via E. Orabona 4, 70126 Bari, Italy*

[ℓ] *COM – Centre d'Océanologie de Marseille, CNRS/INSU Université de la Méditerranée Aix-Marseille II, Station Marine d'Endoume-Luminy, Rue de la Batterie des Lions, 13007 Marseille, France*

[m] *NIKHEF, Kruislaan 409, 1009 SJ Amsterdam, The Netherlands*

[n] *University of Leeds, Department of Physics and Astronomy, Leeds LS2 9JT, United Kingdom*

[o] *Dipartimento di Fisica ed Astronomia dell'Università e Sezione INFN, Viale Andrea Doria 6, 95125 Catania, Italy*

[p] *University of Sheffield, Department of Physics and Astronomy, Hicks Building, Hounsfield Road, Sheffield S3 7RH, United Kingdom*

[q] *Dipartamento di Fisica dell'Università e Sezione INFN, Largo B. Pontecorvo 3, 56127 Pisa, Italy*

[r] *IASF/CNR, 40129 Bologna, Italy*

[s] *UMR GoScience Azur, Observatoire Ocanologique de Villefranche, BP48, Port de la Darse, 06235 Villefranche-sur-Mer Cedex, France*

[t] *IFREMER – Centre de Brest, BP 70, 29280 Plouzané, France*

[u] *IFREMER – Centre de Toulon/La Seyne Sur Mer, Port Brégaillon, BP507, 83500 La Seyne Sur Mer, France*

[v] *IReS – Institut de Recherches Subatomiques, CNRS/IN2P3 et Université Louis Pasteur, BP 28, 67037 Strasbourg Cedex 2, France*

[w] *Université Paris VII, Laboratoire APC, UFR de Physique, 2 Place Jussieu, 75005*

Paris, France

[x] *ITEP – Institute for Theoretical and Experimental Physics, B. Cheremushkinskaya 25, 117259 Moscow, Russia*

[y] *INFN – Labaratori Nazionali del Sud (LNS), Via S. Sofia 44, 95123 Catania, Italy*

[z] *ISS – Institute for Space Siences, 77125 Bucharest – Magurele, Romania*

Abstract

The ANTARES neutrino telescope, to be immersed depth in the Mediterranean Sea, will consist of a 3 dimensional matrix of 900 large area photomultiplier tubes housed in pressure resistant glass spheres. The selection of the optimal photomultiplier was a critical step for the project and required an intensive phase of tests and developments carried out in close collaboration with the main manufacturers worldwide. This paper provides an overview of the tests performed by the collaboration and describes in detail the features of the photomultiplier tube chosen for ANTARES.

Key words: Large area photosensor, Hemispherical photomultiplier, Neutrino detection
PACS: 95.55.Vj, 85.60.Ha

1 Introduction

The ANTARES collaboration is constructing a neutrino telescope [1] to be operated at great depth in the Mediterranean Sea. This telescope is a first step towards a full scale km^3 detector. To this end, during the last years many efforts have been put into R&D studies, especially concerning one of the most crucial components of the detector, the photomultiplier tubes (PMTs). The main results of these tests, performed in close collaboration with PMT manufacturers, are described in this paper.

Section 2 describes the detection principle of a deep-sea neutrino telescope and the layout of ANTARES. The requirements that the photo-sensitive detectors should satisfy and other relevant PMT characteristics are reviewed in section 3. These criteria led to the pre-selection of a limited number of PMT candidates. The results of the main tests performed on these candidates are given in section 4. In the last section, the main features of the PMT chosen for ANTARES, the Hamamatsu R7081-20, are summarised. These results are based on the measurements made on a sample of 912 units purchased and tested in 2001.

2 Detection principle of a neutrino telescope

High energy muon neutrinos can be detected by observing the long-range muons produced by neutrino interactions with the matter surrounding the detector [2]. In a transparent medium, such as water or ice, the Cherenkov light induced by these relativistic muons can be detected by a three-dimensional array of PMTs. The measurement of the arrival time of the Cherenkov light at each PMT combined with the knowledge of their positions allows the reconstruction of the muon direction. The number of photons hitting each PMT gives an estimate of the muon energy.

Though simple in principle, the design of the telescope is limited in practice by two essential constraints:

- A very large muon flux is naturally produced by cosmic ray interactions with the Earth's atmosphere. In order to reduce this background, the neutrino telescope must be located in the sea (or ice) at a depth of a few kilometres. Therefore, the PMTs must be housed in a transparent and pressure-resistant glass sphere. This glass sphere, together with the equipment inside, is called Optical Module (OM).
- Due to the very low flux of high-energy neutrinos from astrophysical sources and to the small neutrino interaction cross-section, a large-volume detector is necessary.

Figure 1 shows a schematic view of the ANTARES telescope. It consists of 12 vertical lines, separated by 60-75 m from each other. Each line is equipped with 75 OMs, in groups of three forming storeys separated by 14.5 m. The whole detector is immersed at a depth of 2500 m and connected to the shore by a 40 km long electro-optical cable.

3 Specifications for the ANTARES photomultiplier tubes

This section describes the specifications required for the photomultiplier tubes used in ANTARES. In order to establish a standard set of measurement parameters, we require the following conditions during the tests:

- an average light level corresponding to well below one photoelectron is used;
- the high voltage is fixed to HV_{nom} (see below);
- the PMT is shielded against the Earth's magnetic field;
- measurements are performed at room temperature ($\sim$20°C);
- the light source illuminating the photomultiplier should have a wavelength of about 450 nm;

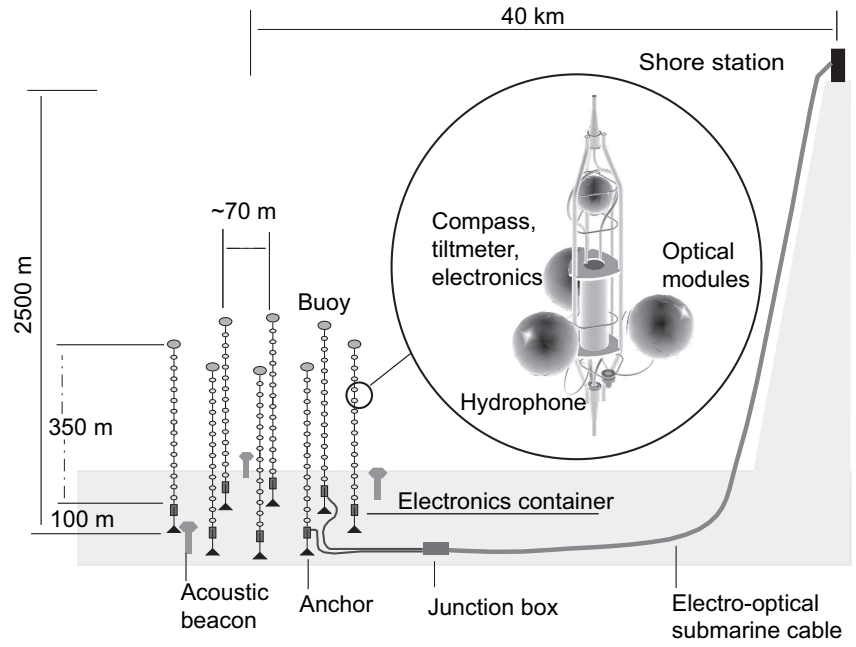

Fig. 1. The ANTARES detector will consist of 12 lines, about 450 m long, out of which 350 m are equipped with 75 optical modules grouped in 25 triplets called storeys.

- the temporal width of the light pulse is lower than 1 ns (FWHM);
- light homogeneously illuminates the photocathode.

- **Dimensions**

  Figure 2 shows a sketch of the ANTARES OM [3]. It consists of a pressure-resistant glass sphere housing the photomultiplier embedded in silicon gel to ensure a good optical coupling. A high permittivity alloy cage surrounds the tube, shielding it against the Earth's magnetic field. Signal outputs and HV control and monitoring are transmitted through pressure-resistant connectors to and from the outside world. The glass sphere, made of two separate halves, is closed by applying an inner under-pressure of 200-300 mbar. The sphere dimension (41.7 cm inner diameter) limits the photocathode diameter to ∼38 cm (15" PMT), and the total PMT length to ∼35 cm.

- **Gain**

  The noise level of the electronic circuit used to digitise the PMT pulse requires a single photoelectron (SPE) amplitude of the order of 50 mV on a 50 Ω load [4]. This requires the photomultiplier gain to be at least 5×10^7. The HV value corresponding to this gain will be called nominal voltage, HV_{nom}, hereafter. The HV_{nom} is not limited in principle, but should remain small enough (<2000 V) to ensure long term stability and avoid ageing problems. Experience shows that these requirements restrict the choice to tubes equipped with at least 10 amplification stages, linear focusing or box-line type.

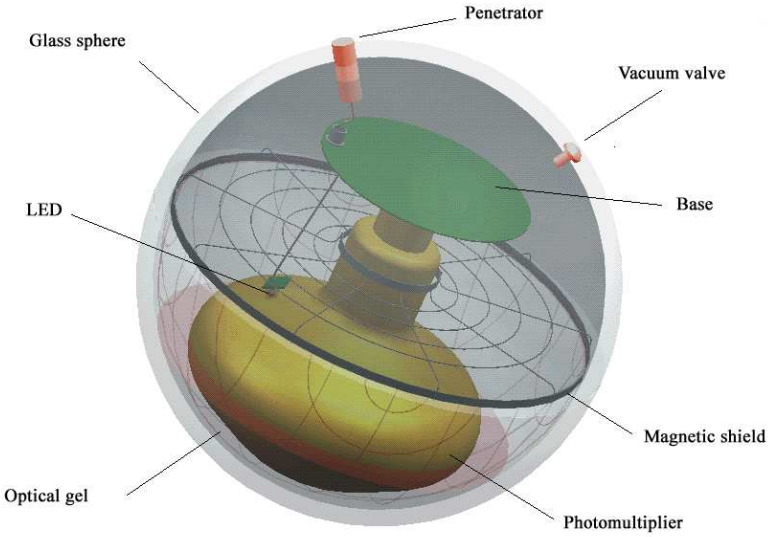

Fig. 2. Sketch of an ANTARES optical module. A large hemispherical photomultiplier (10 inch diameter) is protected by a pressure-resistant glass sphere. The outer diameter of the sphere is 43.2 cm.

- **Peak to valley ratio**

  For an absolute calibration of the telescope, it is necessary to be able to properly isolate a single photoelectron from the pedestal. This requires a peak to valley ratio (P/V) to be at least 2, as computed from the charge spectrum (see section 4 for details).

- **Transit time spread**

  The muon direction is reconstructed from the arrival time of the Cherenkov light at each PMT. The relationship between the required muon angular resolution and the time resolution has been estimated using a full computer simulation, taking into account the effect of all timing uncertainties. Considering that we are aiming at an absolute time calibration better than $\sigma_{cal} = 1$ ns, the timing uncertainty due to the jitter of the PMT response should also remain of the order of 1 ns, in order not to degrade significantly the angular resolution. In the following, the so-called transit time spread (TTS) will refer to the full-width at half maximum (FWHM) of the transit time of the signal in the phototube. This TTS should not exceed 3 ns.

- **Signal shape characteristics**

  In order to be able to separate events which are close in time, the pulse shape must be stable, non saturated and smooth. Moreover, to improve the time resolution and the analysis of the PMT signals, the rise-time (measured between 10% and 90% of maximum), fall-time and pulse width must be shorter than 5 ns, 15 ns and 12 ns, respectively.

Type	Time window	Main pulse	Limit
Prepulses	[-100 ns, 10 ns]	Yes/No	1%
Delayed pulses	[10 ns, 100 ns]	No	5%
Afterpulses type 1	[10 ns, 100 ns]	Yes	1%
Afterpulses type 2	[100 ns, 16 μs]	Yes	10%

Table 1
Definitions and limits (ratio of pulse rate in the time interval over the main pulse rate) for different out-of-time pulses. The time window is defined with respect to t_0. The presence of a pulse in the main pulse window ($t_0 \pm 10$ ns) is also shown.

- **Dark noise**

  The dark noise rate, also known as dark count (DC), does not have a big impact on ANTARES compared to other experiments, because of the important optical background due to natural radioactivity of potassium and bioluminescence. Previous measurements [5] show that the continuous rate of single photoelectron events is about 60 kHz on a 10" photomultiplier[¶].

  The DC is measured at a 0.25 photoelectron threshold level after the PMT has been kept in the dark for two hours. In these conditions, the DC should be less than 10 kHz.

- **Out-of-time pulses**

  Prepulses and afterpulses have several origins which can be disentangled if the time interval that separates them from the main pulse is long enough. Since they are time correlated with the true pulses, prepulses as well as afterpulses can prevent a correct reconstruction or mimic real physical events.

  We call t_0 the mean arrival time of the expected PMT signal associated with the light pulse. The definitions and limits for the different out-of-time pulses we have considered are given in table 1.

- **Photocathode requirements**

  Due to the low density of photomultipliers in the ANTARES telescope (about 10^{-4} PMT/m^3), the photon yield produced by cosmic events on the OMs is very small. Therefore, the photocathode must be as large as possible to minimise the cost of mechanics, within the constraints on the dimensions discussed previously. The geometrical surface of the photocathode should be larger than 500 cm^2. On the other hand, the quantum efficiency should be at least 20% and the collection efficiency at least 80% over the whole photocathode surface.

[¶] PMTs also occasionally detect bioluminescence bursts which produce sudden and short rate excursions at several MHz.

- **Mechanical and environmental strength**

  The rather peculiar environment of the photomultipliers has to be taken into account in defining their specifications. The photomultipliers should be able to bear vibrations of up to 1 g and 1 to 55 Hz, produced during transport and deployment (boat, deck, etc.). They should also withstand temperature variations from -10°C to +60°C. Once in place, the tubes will stay in a rather quiet surrounding at a constant temperature (∼13°-14°C).

There are other features which are not considered specifications but are of interest to characterize the tubes. The energy resolution is a useful parameter to estimate the fluctuations in charge of the SPE events. A value below 40% is considered good enough for this kind of photomultipliers. The effective area, A_{eff}, is defined as the product of the surface of the photocathode by the collection efficiency. It should be as large as possible. Finally, the effect of ageing has also to be measured. The telescope is designed for a lifetime of about 10 years and the total charge delivered to the anode is expected to be 0.1-0.2 C/day for each PMT. Although recovery and repair of the elements of the detector is possible, this is a costly operation. Therefore, the PMTs should have a good stability and a long lifetime.

4 Comparison of PMT candidates

A large variety of PMT models have been tested and characterized taking into account the constraints listed in the previous section. Tubes considered by ANTARES either already existed on the market or have been developed recently and specifically for neutrino telescopes. In this case, their tests were carried out by ANTARES in close collaboration with the manufacturers.

Among the available models, we chose those closest to the specifications: the 10" Hamamatsu R7081-20, the 10.6" Photonis XP1804/D2 and the 13" Hamamatsu R8055. Table 2 lists the characteristics of these tubes. In the following, detailed results of the measurements performed on these PMTs are presented.

4.1 Experimental setup

In this section, the experimental setup used at IFIC (Valencia) during the selection stage is described. For a description of the setup at CEA/DAPNIA (Saclay) see section 5, where the results obtained on the whole sample of R7081-20 are presented.

Model	Photocathode diameter	Number of stages	Dynode structure
Hamamatsu R7081-20 [6]	10”	14	Box line
Photonis XP1804/D2 [7]	10.6”	11	Linear focused
Hamamatsu R8055 [6]	13”	10	Box line

Table 2
List of the PMT candidates studied by ANTARES.

As it can be seen in figure 3, the photomultiplier is set in a black box (80 cm $\times$ 80 cm $\times$ 140 cm) in order to protect it from the environmental light. A μ-metal cage shields it against the Earth's magnetic field. The HV is supplied by a NIM module located in the crate outside the box. The photomultiplier is illuminated by means of a green laser located in another black box and triggered by a pulse generator. An optical fibre guides the light from the laser into the PMT black box. In order to get uniform illumination of the whole photocathode an Oriel 48020 diffuser [8] is used at the end of the optical fibre at a distance of about 80 cm from the PMT head. Depending on the measurement being performed, the output signal from the photomultiplier is sent either to NIM and CAMAC modules or to a digital oscilloscope (Tektronix TDS640A [9]). Both the CAMAC modules and oscilloscope are read out through a GPIB link by a LabView program running on a PC.

The green laser used as light source to illuminate the photomultiplier is a Nd-YAG device[‖], i.e. a synthetic ($Y_3Al_5O_{12}$) crystal doped by Nd in concentrations of 10^{20} atoms/cm^3. It is pulsed by the Q-switching mechanism, providing very fast pulses ($\sigma \leq$0.5 ns). The emitted energy per pulse is $\sim$1.2 μJ. The output stability is better than 1% over several hours and the energy emission changes less than 1% after switching on and off. The emission wavelength is 532 nm. An internal photodiode located in its head provides a trigger signal with an error smaller than 50 ps.

4.2 PMT comparison

The following quantities were measured for each of the 3 PMT candidates: gain, amplitude, peak to valley ratio, energy resolution, transit time spread, dark noise rate and out-of-time pulse rate. Much of this information (gain, peak/valley, energy resolution) is obtained from the SPE charge spectrum. This distribution can be described by

[‖] The laser model is NG-10120-120 from Nanolase [10]

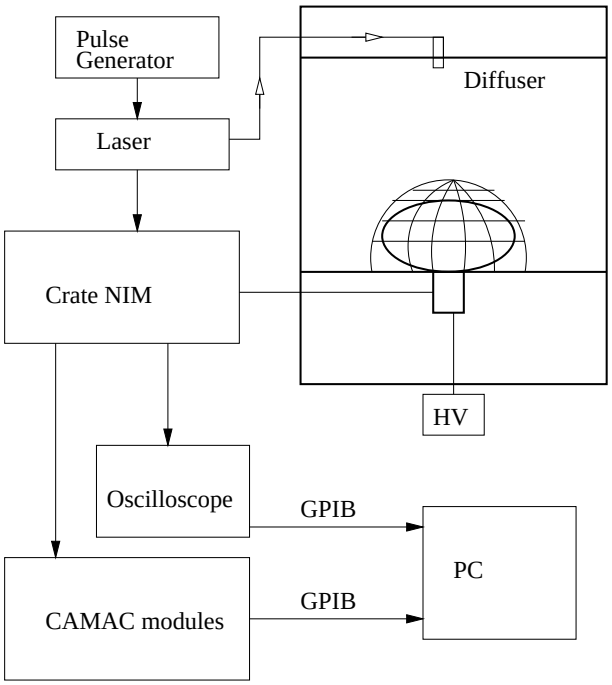

Fig. 3. Schematic view of the experimental setup. The photomultiplier is inside a black box. A μ-metal cage is used in order to shield it from the Earth's magnetic field. The laser is pulsed by means of a pulse generator and its light is guided via a fibre optical cable inside the black box and diffused there to illuminate homogeneously the PMT. The acquisition is performed by CAMAC modules or an oscilloscope (depending on the measurement) and the data are sent to a PC via GPIB.

$$S(q) = G_p(q; \mu_p, \sigma_p) + F(q; \omega, \alpha, \beta) + \sum_{n=1}^{\infty} P(n; \mu) \times G_n(q; \mu_n, \sigma_n), \qquad (1)$$

where G_p and G_n are the Gaussian distributions corresponding to the pedestal and to n photoelectrons respectively and F is the valley function. The valley is approximated by the sum of an exponential and a Gaussian. Three parameters are needed to describe this phenomenon: the fraction of badly amplified photoelectrons ω, the fraction of valley events contributing to the exponential (and not to the Gaussian) β and the "slope" of the exponential α. P is the Poisson probability of producing n photoelectrons at the first dynode if the product of the number of photoelectrons emitted at each laser shot, the quantum efficiency and the collection efficiency is μ. If μ_1 and σ_1 are the parameters of the Gaussian for a single photoelectron reaching the first dynode, the corresponding parameters for two or more (n) photoelectrons are $\mu_n = n \cdot \mu_1$ and $\sigma_n^2 = n \cdot \sigma_1^2$.

Therefore, there are 8 free parameters $(\mu, \mu_p, \sigma_p, \mu_1, \sigma_1, \omega, \alpha, \beta)$ that can be obtained fitting the measured charge spectrum to equation 1. A typical example of a charge spectrum is shown in figure 4.

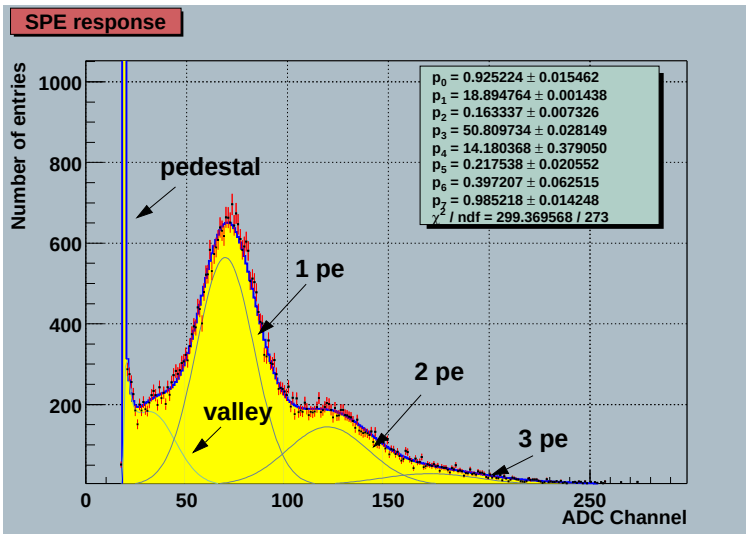

Fig. 4. Example of charge spectrum. Each of the contributions described in the text is shown separately. Each channel of the ADC corresponds to 0.25 pC.

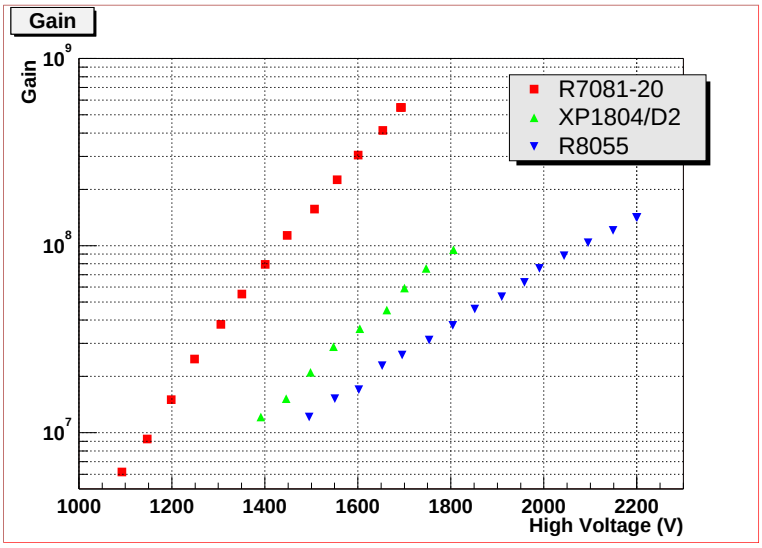

Fig. 5. Gain dependence on HV for the three candidate photomultipliers.

4.2.1 Gain

The gain is obtained from the position of the SPE peak in the charge spectrum. Figure 5 shows the gain dependence on HV for the three candidates. From these plots, the nominal voltage can be determined: 1340 V for the R7081-20, 1680 V for the XP1804/D2 and 1900 V for the R8055.

The highest gains are reached by the Hamamatsu R7081-20 model, as expected since this tube has 14 dynodes. It was designed to attain gains in excess of 10^9, required by some experiments to transfer the analogical PMT signal along km-long electric cables (AMANDA [13]). In the case of the Photonis XP1804/D2, which has only 11 dynodes, the nominal voltage is naturally higher and the

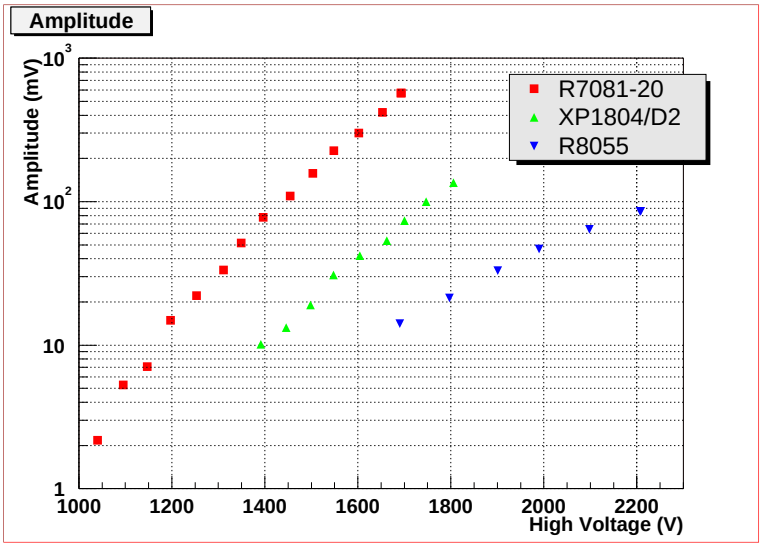

Fig. 6. Amplitude dependence on HV for the three candidate photomultipliers.

increase in gain with HV smaller than for the R7081-20 model. Finally, the Hamamatsu R8055 needs an even higher voltage to reach the nominal gain. This is not surprising since the HV division for this tube was optimized for TTS and not for gain. As we will see later, all 3 PMTs are able to reach a gain of 10^8 without significant deterioration of their properties.

4.2.2 Amplitude

The experimental setup used to obtain the SPE amplitude distribution is similar to that used for the charge spectrum measurement. In this case, the acquisition is performed by a digital oscilloscope.

The fitting procedure is simpler than in the previous case. The SPE peak is fitted to a Gaussian, whose mean is the amplitude. Figure 6 shows that the dependence of the amplitude on HV is very similar to that of the charge. This is to be expected since for a given PMT, amplitude and charge are nearly proportional and related to the pulse shape which in turn is linked to the dynode structure of the photomultiplier. It is important to note that in the ANTARES experiment, the signal amplitude will be used in the trigger (see [4] for a more detailed description).

The typical SPE amplitudes between anode and ground on 50 Ω at the nominal voltage are 46, 60 and 34 mV respectively for the R7081-20, the XP1804/D2 and the R8055.

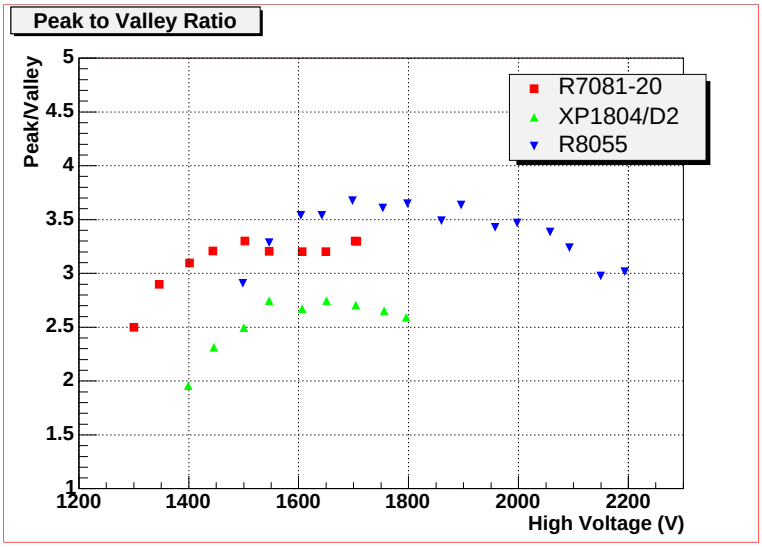

Fig. 7. Peak to valley ratio dependence on HV for the three candidate PMTs.

4.2.3 Peak to valley ratio

The ratio between the height of the SPE peak and the valley, measured from the SPE charge spectrum, is important since it can be used to estimate the capability of the photomultiplier to discriminate the number of photoelectrons in an event. As it was seen in section 3, the ANTARES specifications require a P/V larger than 2. Figure 7 shows the results of the measurements for this quantity.

The peak to valley ratio of the Hamamatsu R7081-20 model at the nominal voltage is around 2.8. For higher HV, it is almost flat in the region of interest. Concerning the Photonis photomultipliers, it can be seen that the P/V ratio is around 2.7. It grows with HV at low voltages and then levels off. The peak/valley ratio of all the Hamamatsu R8055 tubes is very good (P/V=3.7) and stable near the nominal voltage. For very low or very high voltages, the peak/valley ratio decreases.

4.2.4 Energy resolution

Energy resolution is calculated as the ratio of σ_1 to μ_1. The results are shown in figure 8.

The 10" Hamamatsu model exhibits an almost flat dependence on HV. The behaviour of the XP1804/D2 is also smooth. There is a slow increase of the energy resolution with HV, which becomes stable near the nominal voltage. At this point, energy resolution is in general over 30%. In the curve corresponding to the R8055, two regions can be observed: the energy resolution undergoes a relatively fast increase at low voltages and then stabilises. Table 3 shows the

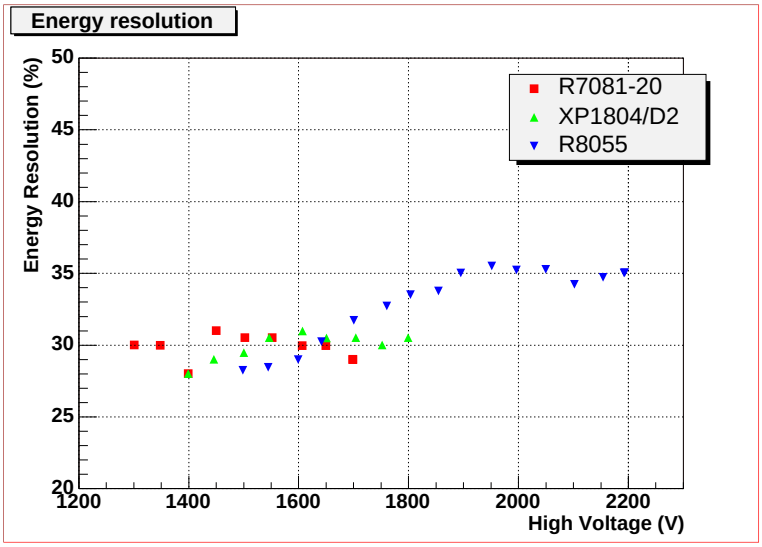

Fig. 8. Energy resolution dependence on HV for the three candidate PMTs.

energy resolution at the nominal voltage.

4.2.5 Transit time spread

As already pointed out, the transit time spread is a key parameter and has to be measured with high accuracy. The setup for this measurement is as follows. The laser illuminates the photomultiplier, whose output is discriminated in order to provide the STOP signal to the TDC. The START signal is given by the internal photodiode of the laser. The results presented in this section were obtained setting the discrimination threshold at 0.5 pe. The total FWHM consists of three components: $\Gamma^2 = \Gamma_P^2 + \Gamma_L^2 + \Gamma_e^2$, where Γ_P is the intrinsic TTS of the photomultiplier that we aim to measure, Γ_L is the FWHM of the laser pulse and Γ_e is the time jitter contribution from the electronics. In order to subtract the two last terms, a very fast photomultiplier was used. Hamamatsu indicates for this photomultiplier (model R5496) a value of FWHM $= 0.23 \pm 0.01$ ns. Illuminating the fast photomultiplier using the same experimental setup it is possible to measure the total width of the distribution Γ and calculate the effect of the source and the electronics. Our measurement shows that they contribute as much as 0.65 ± 0.05 ns to the total FWHM.

The dependence of the TTS on HV is shown in figure 9. As expected, the TTS decreases for higher voltages. This behaviour is nearly the same for all three candidates, with a decrease of about 1 ns for a 300-400 V change around the nominal voltage.

As in the case of the charge spectrum, the errors given by the fit are much smaller than those due to fluctuations in the experimental conditions, so that an estimate of the latter is obtained by repeating the measurements. The best

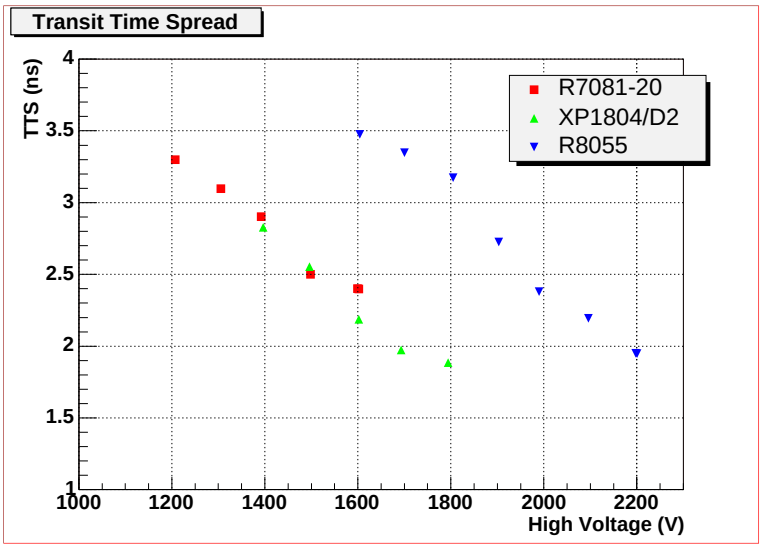

Fig. 9. TTS dependence on HV for the three candidate photomultipliers.

values of TTS are obtained for the Photonis PMT. However, all the models provide results within the chosen specifications.

4.2.6 Dark noise

To measure the dark current, the output from the photomultiplier is sent to a Linear Fan In / Fan Out module that sends identical signals to amplitude discriminators. The number of pulses above each threshold is counted. Each discriminator uses a different threshold. For the sake of comparison among the tubes, this threshold is expressed in number of photoelectrons in amplitude.

The dependence of the dark noise on HV has been measured using this setup. The results are plotted in figure 10, where the dark noise rate for a threshold of half a photoelectron is shown.

Whereas the dark noise dependence on the HV for the 10" Hamamatsu PMT is almost flat, it increases smoothly for the other two tubes. This increase is faster at low voltages for the 10.6" Photonis PMTs, while the opposite occurs for the 13" Hamamatsu tubes, where the increase is faster at high voltages.

4.2.7 Out-of-time pulses

As it has been mentioned, it is important to control out-of-time pulses since it may cause misreconstruction problems. Several kinds of events have been analyzed.

The experimental setup used to measure the out-of-time pulse rate is similar to that used to measure the SPE spectrum. The photomultiplier is illumi-

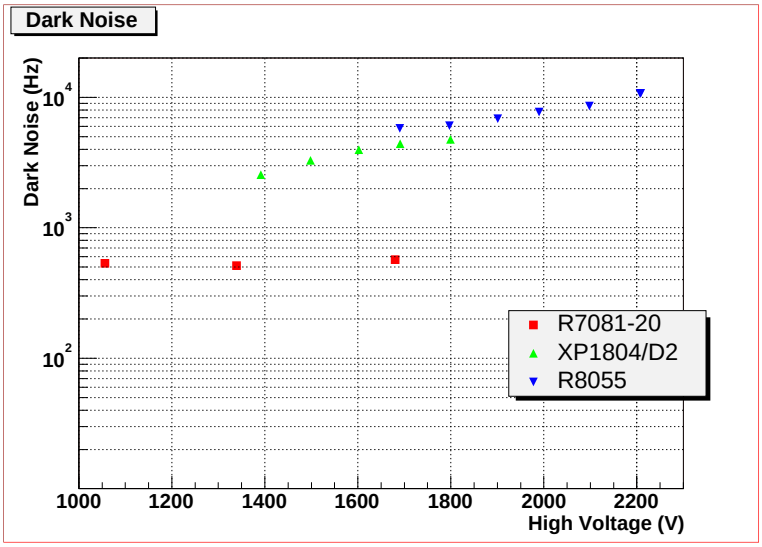

Fig. 10. Dark noise rate dependence on HV. A threshold of half a photoelectron has been used.

nated by a low level of light (∼0.1 pe per pulse) and its output is sent to the oscilloscope, which is triggered by the laser internal photodiode. The oscilloscope digitizes the output from the PMT and sends it to the PC, where a LabView program finds the peaks in the waveform. The time scale used in the analysis of prepulses, delayed pulses and afterpulses-1 is 0.2 ns per channel which allows to cover ±200 ns around the main pulse. On the other hand, the scale to measure afterpulses-2 is 10 ns per channel, i.e. it covers the region from −4 to 16 μs with respect to the main pulse window. In this case, the signal from the photomultiplier is too narrow to be detected by the oscilloscope. A discriminator is used, which implies, however, a loss of the amplitude information.

The R7081-20 is within the specifications. The XP1804/D2 shows a high rate of afterpulses-1 and -2. Some of the rates for the R8055 are also high (see table 3).

4.2.8 Photocathode effective area

As mentioned in section 3, the effective area is the surface of the photocathode multiplied by the collection efficiency, which is often dependent on the hit position. This dependence is estimated by scanning the PMT with a collimated LED, assuming the collection efficiency to be near unity at the very centre of the photocathode.

As expected, the best value of the effective area corresponds to the larger PMT, i.e. the Hamamatsu R8055. The smallest effective area is that of the Photonis XP1804/D2, although being a bit larger in diameter than the Hamamatsu

Model	Specification	R7081-20	XP1804/D2	R8055
Nominal Voltage (V)	$\leq$2000	1340	1680	1900
Peak/Valley	≥ 2	2.8	2.7	3.7
TTS (ns)	$\leq$3	3.0	2.0	2.6
Dark Noise (Hz)	$\leq$10000	910	9200	8100
Prepulses (%)	$\leq$1	0.01	0.01	2.2*
Delayed pulses (%)	$\leq$5	3.6	4.7	5.0
Afterpulses-1 (%)	$\leq$1	1.0	3.2*	2.4*
Afterpulses-2 (%)	$\leq$10	3.8	18*	19*

Table 3
Comparison of the specifications and measured values (at a gain of 5×10^7) of the parameters of the three candidate photomultipliers. TTS and dark noise are measured with a threshold of 0.25 pe. The definitions of the out-of-time pulses are given in the text. The symbol * indicates that the value is outside the specifications.

R7081-20.

4.3 Conclusions on comparison

Tables 3 and 4 summarize the value of the measured parameters. All the candidates present good performance in general. All PMTs have good values for gain (the nominal voltage is lower than 2000 V and the gain reaches 10^8). The peak to valley ratio for all the models is well in agreement with our requirements for all the models, being always above 2. The values of the energy resolution are similar, and all within the specifications. Concerning the transit time spread, the XP1804/D2 shows the lower value of TTS, the values for R7081-20 and R8055 being also acceptable. The best value of dark noise is achieved by the R7081-20 (better than expected given its smaller photocathode). The other two models are also within the specifications. Both XP1804/D2 and R8055 present high afterpulse rates and the latter has also a high prepulse rate. The PMT with a best ratio of the photocathode effective area to the photocathode surface is the Hamamatsu R7081-20. Finally, the Hamamatsu R7081-20 model was chosen for the ANTARES detector.

5 Hamamatsu R7081-20

The results presented in this section correspond to the final sample of 912 PMTs of the Hamamatsu model R7081-20 which have been characterized in

Model	R7081-20	XP1804/D2	R8055
Amplitude (mV)	46	60	34
Energy Resolution (%)	30	31	35
Effective Area (cm^2)	450	410	830

Table 4
Other features of the studied tubes, not considered as specificaions.

the ANTARES test bench at CEA/DAPNIA, Saclay.

Given the high number of PMTs involved, the experimental test setup has to allow all measurements to be performed at a fast rate. The test bench consists of a light tight plastic cylinder 1.5 m long and 0.46 m in diameter. The cylinder was painted in black on the inside to avoid reflections and covered by a μ-metal foil externally. Light from a pulsed blue LED is fed through an optical fibre into one extremity of the tube. A Lambertian diffuser (Oriel 48010 [8]) located just after the LED and about 1.1 m away from the PMT is used to ensure uniform illumination of the whole photocathode. The PMT itself is shielded by a μ-metal cage that reduces the Earth's magnetic field by a factor 3 to 4. Instead of the PMT base provided by Hamamatsu, a new base (a modified version of the PHQ5912 base developed by ISEG [14]) was used. The HV and the distribution for the dynodes is generated by the base itself. This change also allowed some improvement in the PMT response, in particular in the TTS. Due to this new design, the results given in this section for the R7081-20 model slightly differ from those given in section 4. A summary of the results of the parameters studied for this sample of PMTs is shown in Table 5.

Finally, in order to study the ageing of the selected model, three tubes were placed in a black box and excited by three independent blue LEDs located a few centimeters above the top of the PMTs. LEDs were tuned to reproduce the optical background environment (^{40}K and bioluminescence) expected in the ANTARES site [5]. In a first run, the LEDs were programmed to emit a continuous rate of 100 kHz and bursts of 1 MHz lasting 0.1 second every second. The total integrated charge in the PMTs amounts to more than 100 C, which corresponds to two years in the sea at a constant gain of 10^8. Subsequently, the LED pulse rate was increased by a factor of 5, thus allowing a total charge of 500 C, corresponding to 10 years in the sea, to be collected by the PMTs. The most significant variation of the PMT properties concerns the gain. Over the first 100 days, all three PMTs showed an increase of 50-70% in gain, before they level off. This phenomenon corresponds to the runnning-in phase, rather than ageing. All other important energy and timing properties of the PMTs (P/V, energy resolution and TTS) were stable over the test period. The dark current remained also stable with time. However, afterpulse-2 rate showed an increase (around 30%) during the test, possibly caused by the fact that these pulses are usually due to gas of ionized atoms, whose number increases with

Parameter	Mean	RMS
Nominal Voltage (V)	1804	57
Amplitude (mV)	42.7	2.3
Peak/Valley	2.79	0.46
TTS (ns)	2.79	0.15
Raise Time (ns)	4.30	0.10
Fall Time (ns)	12.57	0.74
Time width (ns)	7.48	0.35
Dark Noise (Hz)	1880	1078
Prepulses (%)	0.010	0.014
Delayed pulses (%)	3.71	0.24
Afterpulses-1 (%)	1.50	0.27
Afterpulses-2 (%)	1.23	0.44

Table 5
Mean and RMS of the distributions of several parameters for the 912 Hamamatsu R7081-20 PMTs.

time.

6 Conclusion

The ANTARES collaboration has carried out a study of large cathode photomultipliers for a submarine neutrino telescope. Several candidates have been considered. In particular, intensive tests on the R7081-20 and R8055 models from Hamamatsu and the XP1804/D2 from Photonis have been performed. The measurements to compare them show that they have in general appropriate performance. Finally, the R7081-20 model was chosen for the contruction of the ANTARES neutrino telescope and the full quantity of 912 PMTs supplied were tested. The measurements on this batch show that the mean values are within the specifications (only the average afterpulse-1 rate is slightly over the limit). The tubes which are not within the specifications are few and close to the limits. Nevertheless they were replaced.

References

[1] E. Aslanides et al., ANTARES collaboration, IFIC/99-42 and astro-ph/9907432.

[2] M. A. Markov, Proceedings of the Rochester Conference, New York (1960).

[3] P. Amram et al., ANTARES collaboration, Nucl. Instr. and Meth. in Phys. Res., A **484** (2002) 369-383.

[4] F. Feinstein for the ANTARES Collaboration, Proc. 2002 Conference on advances in Photon Detection, Beaune, France, July 2002.

[5] P. Amram et al., ANTARES collaboration, Astrop. Phys. **13** (2000) 127-136.

[6] Hamamatsu Photonics K.K., http://www.hamamatsu.com.

[7] Photonis Imaging Sensors, http://www.photonis.com.

[8] Thermo Oriel Co., http://www.oriel.com.

[9] Tektronix. Tektronix TDS620A, TDS640A, TDS644A Digitalizing Oscilloscopes. User Manual.

[10] JDS Uniphase Co., http://www.nanolase.com.

[11] Hamamatsu Photonics K.K., Photomultiplier tubes, 1994.

[12] F. James, MINUIT Function Minimization and Error Analysis, CERN Program Library, entry D506.

[13] E. Andres *et al.*, AMANDA collaboration, Astropart. Phys. **13** (2000) 1.

[14] ISEG Spezialelektronik GmbH, http://www.iseg-hv.com.